ELSEVIER

Thin Solid Films 377–378 (2000) 425–429

thin solid films

www.elsevier.com/locate/tsf

A structural and mechanical analysis on PVD-grown (Ti,Al)N/Mo multilayers

C.J. Tavares[a,*], L. Rebouta[a], E. Alves[b], A. Cavaleiro[c], P. Goudeau[d], J.P. Rivière[d], A. Declemy[d]

[a] *Departamento Física, Universidade do Minho, Azurém, 4800-058 Guimarães, Portugal*
[b] *Departamento Física, ITN, E.N. 10, 2686-953 Sacavém, Portugal*
[c] *ICMES, F.C.T da Universidade de Coimbra, 3030 Coimbra, Portugal*
[d] *Laboratoire de Metallurgie Physique, Université de Poitiers, 86960 Futuroscope, France*

Abstract

(Ti,Al)N/Mo multilayered hard coatings have been designed to fulfil future applications concerning wear-prevention on tool steels. They have been deposited by reactive dc magnetron sputtering on high-speed steel substrates with modulation periods between 6.5 and 8 nm. Experimental X-ray diffraction (XRD), Rutherford backscattering spectrometry (RBS) and computational modelling of those patterns has undergone to survey structural properties such as modulation periodicity, interfacial roughness and density. Asymmetric XRD measurements confirmed that the textured grains, although being randomly distributed, possess a slight misorientation of $\pm 11°$ due to their mosaic structure. Atomic force microscopy (AFM) analysis revealed a dome-rounded structure with columnar grain sizes between 90 and 120 nm in diameter, depending on deposition process parameters. The average ultramicrohardness of these multilayers can be as high as 36 GPa with a maximum Young's modulus of 445 GPa, while the adhesion critical load may reach 60 N. © 2000 Elsevier Science B.V. All rights reserved.

Keywords: TiAlN; Mo; Multilayers; Hard coatings; AFM; Hardness; Adhesion

1. Introduction

The physical properties of multilayers are ruled by the amount of structural imperfections inside them. Stacking faults, thickness variations, interface waviness, amongst other factors, contribute to the destruction of the desired perfection [1,2]. Several publications mention the fact that these structures are interesting for tribological applications owing to their elevated hardness and strength [3–5]. Moreover, the tailoring of a multilayer coating can meet specific requirements. Such examples would be the modulation period, relative thickness of the multilayer constituents and roughness.

In this work, we combined XRD and RBS measurements on (Ti,Al)N/Mo multilayer thin films in order to study their structural parameters with the aid of modelling. Furthermore, the misorientation of the textured grains was probed through XRD asymmetric experiments. AFM analysis provided us the surface roughness as a function of the lateral length scale and an estimation of the columnar grain size. Ultramicrohardness experiments yielded both the hardness and the Young's modulus of these coatings. A correlation between the structural and the mechanical properties is given.

2. Experimental details

$[(Ti,Al)N/Mo] \times 100$ coatings were deposited using a custom-made sputtering system; the last layer to be deposited was one of Mo. An Ar/N_2 atmosphere was present in the chamber with a nitrogen flow rate (pres-

* Corresponding author. Tel.: +351-253-510154; fax: +351-253-510153.
E-mail address: ctavares@fisica.uminho.pt (C.J. Tavares).

0040-6090/00/$ - see front matter © 2000 Elsevier Science B.V. All rights reserved.
PII: S0040-6090(00)01269-4

Table 1
Deposition parameters and structural and mechanical results relative to the $[Ti_{0.4}Al_{0.6}N/Mo] \times 100$ multilayers[a]

Sample	P_{Ar}(TiAlN/Mo) (Pa)	Bias (V)	Λ(XRD/RBS) (nm)	t_{TiAlN}/t_{Mo} (XRD/RBS)	σ (TiAlN/Mo) (nm)	HV (GPa)	E (GPa)	L_c (N)	Grain size (nm)	Ra (nm)
E12	0.35/0.5	−80	6.8/6.6	0.45/0.61	1.2/0.4	29 ± 2	366 ± 20	21 ± 1	110	4.4
E13	0.35/0.5	−60	6.6/6.1	0.61/0.61	0.8/0.2	36 ± 5	445 ± 60	54 ± 2	100	3.9
E14	0.35/0.6	−60	7.6/7.4	0.58/0.57	0.9/0.3	31 ± 3	387 ± 19	58 ± 3	120	4.5
E15	0.35/0.6	−80	7.6/7.4	0.65/0.57	1.4/0.4	–	–	–	–	–
E16	0.3/0.5	−60	7.9/7.4	0.65/0.57	0.9/0.1	29 ± 1	379 ± 21	23 ± 2	90	3.0

[a] P_{Ar}(TiAlN/Mo) is the used argon partial pressure to grow TiAlN and Mo, Λ is the modulation period calculated from both refinements of the XRD and RBS patterns, t_{TiAlN}/t_{Mo} is the thickness ratio between TiAlN and Mo, as determined by XRD and RBS, σ is the calculated interfacial roughness at the TiAlN and Mo interfaces, HV is the ultramicrohardness, E is the Young's modulus, L_c is the critical load and Ra is the roughness parameter for a 5 μm × 5 μm AFM scan.

sure) of 5 cm^3/min (0.1 Pa) for growing (Ti,Al)N; the working Ar pressure to grow (Ti,Al)N and Mo is presented in Table 1. Pure 200 mm × 100 mm × 6 mm TiAl and Mo targets were used with a current density applied to both magnetrons of approximately 0.01 A/cm^2. Substrate bias voltages of −60 to −80V were used while the target-to-substrate distance was kept at 65 mm for all depositions. The base pressure was typically of the order of 5×10^{-5} Pa, with a substrate temperature during deposition of 250°C. Before deposition the substrates were in situ sputter etched in an argon atmosphere of 7 Pa with a dc power of 100 W for 20 min. Two types of substrates were used: silicon wafers (100) oriented for RBS and XRD measurements, and high-speed steel (AISI M2) for mechanical testing. Five samples have been elaborated with the deposition conditions given in Table 1.

Rutherford backscattering spectrometry (RBS) was used to determine the film composition. A 2-MeV He^+ beam in a 3.0-MV Van de Graaff accelerator [6] analysed the samples deposited on Si wafers. The backscattered particles were detected by a surface barrier detector placed at 160° to the beam direction in the Cornell geometry and with an energy resolution FWHM of 14 keV and a beam spot of 0.2 mm × 0.6 mm. The RBS spectra were fitted with the RUMP code [7].

For the XRD scans a classical two-circles diffractometer working with Cu K_α radiation was used for both low-angle and high-angle diffraction experiments with the standard Bragg–Brentano geometry. The specular resolution was 0.002° and the integration time 5 s with a 2θ step of 0.01°. In the symmetric low-angle regime, the length scales that are probed are greater than the lattice spacing of the constituent layers. Therefore, the scattering solely arises from the chemical modulation of the structure. The modulation period can be assessed through the position of the small-angle Bragg diffraction peaks [8]:

$$n = \frac{2\Lambda}{\lambda}\sqrt{\cos^2(\theta_c) - \cos^2(\theta_n)} \quad (1)$$

where n represents the order of diffraction related to the Bragg peak positioned at θ_n; Λ is the modulation period of the multilayer; λ corresponds to the radiation wavelength; θ_c is the critical angle (~0.4° for our samples and Cu K_α) below which all radiation is totally reflected. By modelling the low-angle XRD patterns with Suprex [1,9] structural information regarding the relative density and thickness of each material in a bilayer and the interfacial roughness is accessed [10].

The symmetric high-angle XRD scans besides providing the information regarding texture and microstructure give also a confirmation on the modulation period by the position of any given couple of satellite peaks (indexed as a and b) about the multilayer's preferential growth direction:

$$\Lambda = \frac{(a-b)\lambda}{|2(\sin\theta_a - \sin\theta_b)|} \quad (2)$$

In the asymmetric mode, α–2θ scans, the incident angle α is fixed for a particular value while the detector probes a specific 2θ region. The diffraction vector $\boldsymbol{q}$ has a misorientation angle given by $\Psi = \alpha - \theta_B$ with respect to the surface normal. θ_B is the Bragg position for the particular family of (hkl) planes to be investigated and Ψ the angle between the normal to the sample surface and the ⟨hkl⟩ direction. By this method, fibre texture phenomenon may be probed when plotting the maximum intensity corresponding to θ_B as a function of Ψ [11].

A Digital Instruments NanoScope III atomic force microscope (AFM), working in tapping mode, was employed to study the surface morphology of these coatings.

Depth-sensing measurements allow the estimation not only of the hardness but also the Young's modulus [12,13]. The ultramicrohardness experiments were carried out on a computerised Fischerscope dynamic ultramicrohardness tester (H100 model), using a Vickers indenter and a maximum load of 30 mN.

An established method of assessing the adhesion of

hard coatings made by PVD is the scratch test. The equipment used was a Sebastian-5A model from the Quad Group. A 200-μm-radius diamond tip was used with the scratching speed being set at 0.0167 cm/s while the load rate was kept at 100 N/min. An analysis of the AE spectrum coupled with careful microscopic analysis of the scratch tracks aids the identification of the value of the critical load (L_c) [12,14]. We consider L_c as the load at which the first adhesive failure mode occurs and is clearly visible, regardless if the film remains bonded after this incident along the segueing scratch track.

3. Results and discussion

RBS simulations extracted the composition and areal atomic density (atoms/cm^2) of (Ti,Al)N and Mo thick samples. From this result it was assumed that the (Ti,Al)N layers consist of 30 at.% of aluminium, 20 at.% of titanium and approximately 50 at.% of nitrogen, hence we have $Ti_{0.4}Al_{0.6}N$. According to the literature [15], and from the XRD analysis of a thick sample, this stoichiometry evidences a NaCl type structure. To derive the volume density of (Ti,Al)N (4.0 g/cm^3) and Mo (10.2 g/cm^3) we divided the calculated areal atomic density by the film's thickness. RBS experiments on multilayers were performed with tilts of 80°, 83° and 85° in order to determine the thickness of the underlying individual layers with the best resolution. As an example to this, in Fig. 1 the RBS data was collected for three different samples with a tilt of 83°. Despite that only the layers close to surface are actually analysed it is clear by the positioning of the valleys and peaks that the modulation period increases a bit from E13 to E15. With the atomic volume densities ($\rho_{TiAlN} = 9.9 \times 10^{22}$ atoms/cm^3, $\rho_{Mo} = 6.4 \times 10^{22}$ atoms/cm^3) it is possible to calculate the thickness of the individual layers in nm and subsequently the modulation periodicity, using the atomic volume densities. These modulation periods are shown in Table 1 for a better comparison with the following XRD analysis.

The modulation periodicity was determined for all samples with Eq. (1) and coincided with the ones applying to Eq. (2). As for the relative thickness of $Ti_{0.4}Al_{0.6}N$ to Mo (t_{TiAlN}/t_{Mo}) in a bilayer, it was calculated through the refinement with Suprex and compared with the RBS data. These structural results are presented in Table 1. The t_{TiAlN}/t_{Mo} parameters taken from both techniques slightly diverge, which is probably due to the fact that in the thickness calculations with the RBS data the density values that were used are certainly higher than the real ones. In fact, from the XRD low-angle refinements the density of the $Ti_{0.4}Al_{0.6}N$ was estimated to be $\sim 90\%$ of the bulk value, with an exception for E14 ($\sim 80\%$). Nevertheless, a good agreement is found from this comparison

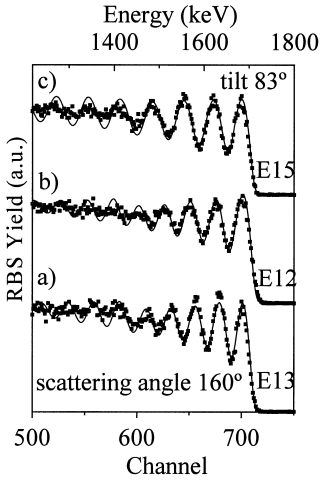

Fig. 1. RBS spectra for a tilt of 83° and corresponding RUMP simulation (full line) for three different samples of [$Ti_{0.4}Al_{0.6}N$/Mo] × 100 multilayers: (a) E13; (b) E12; and (c) E15. Modulation period fluctuations are evidenced by the vertical misalignment of the peaks.

because the error associated with the calculated densities is lower than 10%.

Figs. 2 and 3 show diffraction patterns for low- and high-angle modes. In the first (Fig. 2) the experimental spectra from sample E14 is jointly presented with the calculated one. In this figure, the Bragg peaks are present up to the 8th order, indicating a good chemical modulation. In the high-angle scan from sample E16 (Fig. 3) satellite peaks around the Mo (110) growth direction are resolved. Since the structure factor for Mo is much larger than the corresponding one to $Ti_{0.4}Al_{0.6}N$, instead of having one central peak resulting from the modulation of both materials we have two separated peaks. The peak on the left is associated with $Ti_{0.4}Al_{0.6}N$ (111) and has no satellites due to a smaller structure factor and also to a smaller thickness relatively to Mo in a bilayer. A certain level of internal strain or roughness is present in the film due to the broadening of the satellites. Indeed, the refinement

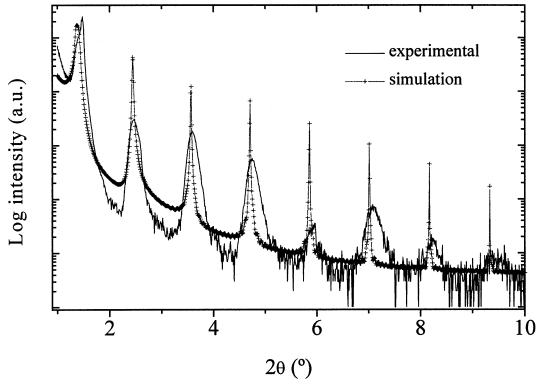

Fig. 2. XRD low-angle spectra and corresponding SUPREX refinement for sample E14 consisting of a 100-bilayer $Ti_{0.4}Al_{0.6}N$/Mo structure with a period of 7.6 nm.

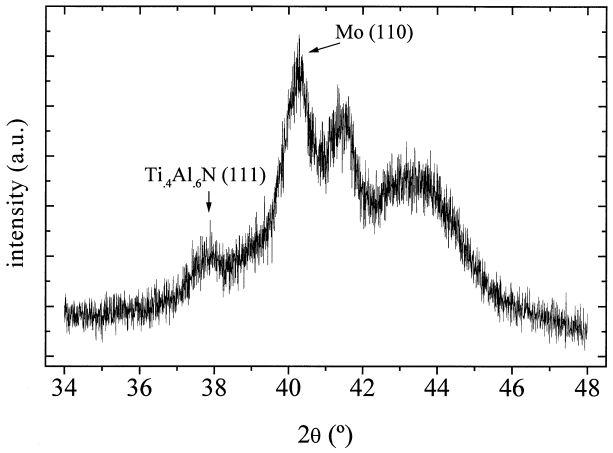

Fig. 3. XRD high-angle spectra for sample E16 consisting of a 100-bilayer $Ti_{0.4}Al_{0.6}N$/Mo structure with a period of 7.9 nm. Satellite peaks are positioned at both sides of the multilayer's preferential growth direction.

procedure with Suprex yielded maximum values of disorder of 1.4 nm. The roughness values at the interfaces from $Ti_{0.4}Al_{0.6}N$ to Mo (σ_{TiAlN}) and from Mo to $Ti_{0.4}Al_{0.6}N$ (σ_{Mo}), which are reported in Table 1, indicate that the first transition is rougher than the second. This is in agreement with the fact that on the left side of the spectra in Fig. 3 the satellite peaks are further masked due to the higher levels of roughness and possible strain within the $Ti_{0.4}Al_{0.6}N$ layers.

Fig. 4 shows asymmetric measurements (α–2θ) made on sample E16 in the diffraction region of $Ti_{0.4}Al_{0.6}N$ (111) and Mo (110). From this, it was possible to conclude that the misorientation level of the $Ti_{0.4}Al_{0.6}N$ (111) fibre axis with respect to the growth direction is important. The value deduced from the Gaussian width of the curve in Fig. 5 is equal to $\pm 11°$. Since Mo is polycrystalline equiaxis a similar analysis was not possible. The level of interfacial disorder, which in a large scale is interpreted as waviness, may explain a reason for such a large tilt in the $Ti_{0.4}Al_{0.6}N$ textured grains. This behaviour is observed in all the samples. From AFM observations this waviness was monitored and its corresponding average roughness (Ra) was calculated from 5 μm $\times$ 5 μm line scans. In Fig. 6 a smaller scan of 0.5 μm $\times$ 0.5 μm is shown for the sample E16. It is possible to observe the dome-rounded shape [16] characteristic of these multilayer columnar grains, which in this particular sample have a diameter of approximately 90 nm. This dome-rounded feature on the surface results from the wavy rough interfaces and texture misorientation of the grains. Hence, AFM roughness results cannot be compared with those derived from the interfaces by modelling the XRD scans due to different sampling lengths (see Table 1). While in the low-angle XRD regime the in-depth coherency length of the X-rays is of the order of a few grains, in the

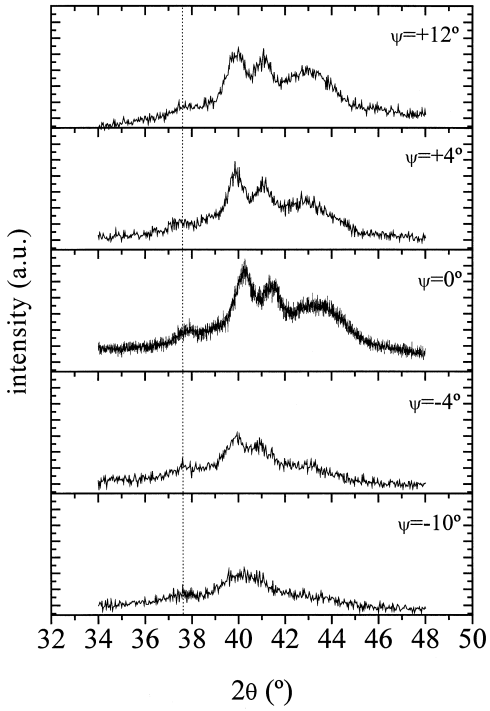

Fig. 4. Asymmetric XRD measurements (α–2θ) made on sample E16 in the $Ti_{0.4}Al_{0.6}N$ (111) diffraction region (dotted line).

AFM case this lateral validity is substantially extended and is essentially on the sample surface. Nevertheless, the XRD roughness data is still useful as a quality control. An increment on the bias polarisation or in the working Ar pressure enhances both values of disorder and columnar grain size. It is well known that an increase in the working gas pressure corresponds to an enhancement of the wave profile of the surface that's being bombarded [17].

A relatively high hardness was found for certain deposition parameters, exceeding 36 GPa in the partic-

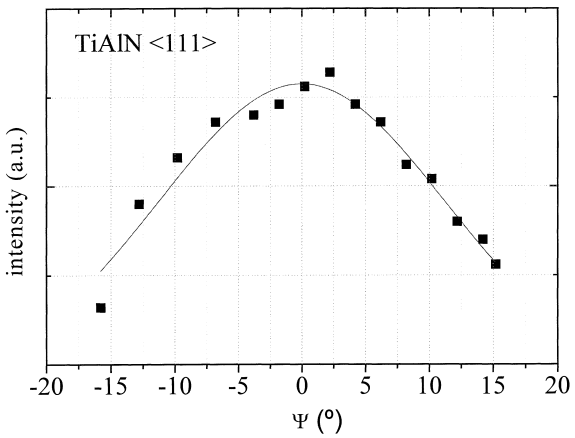

Fig. 5. Variation of the $Ti_{0.4}Al_{0.6}N$ (111) diffraction peak intensity as a function of ψ for sample E16. The width of the Gaussian profile yields a misorientation of $\pm 11°$.

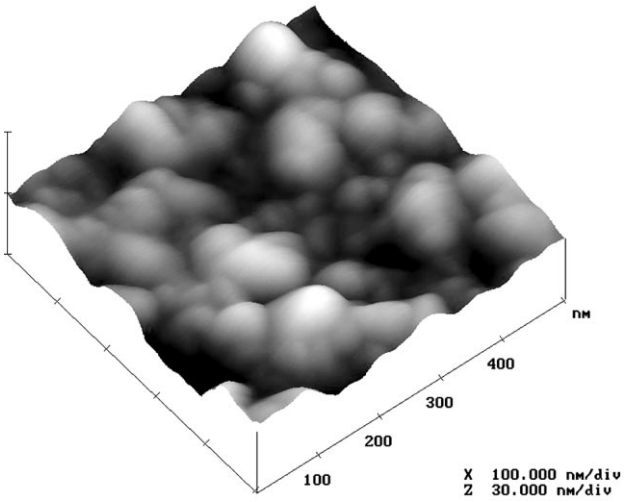

Fig. 6. Atomic force microscopy image of the morphology of sample E16.

ular case of sample E13. Regarding the Young's modulus, it ranged from 366 to 445 GPa, which is also very high. Adhesion critical loads up to approximately 60 N were obtained for the best sample, while the mechanism responsible for the failures is directly related with spallation. From a correlation between hardness, elastic modulus and adhesion results, presented in Table 1, we deduced that a bias voltage of -60 V and working gas pressures of 0.35 Pa and 0.5 Pa for growing $Ti_{0.4}Al_{0.6}N$ and Mo, respectively, yield the best mechanical properties. According to this, a decrease in the energetic bombardment of the growing film and a subsequent decrease of structural disorder enhances the mechanical properties.

These films were produced with the intention of maintaining the modulation periodicity constant throughout the series. However, and due to the PVD process itself, values for Λ ranged from 6.6 to 7.9 nm (see Table 1). Despite this and from what has been concluded, a lower modulation of 6.6 nm produced the highest hardness and Young's modulus.

4. Conclusions

$Ti_{0.4}Al_{0.6}N/Mo$ hard coatings have been produced with optimum levels of hardness, Young's modulus, and adhesion strength to the substrates. From XRD and RBS experiments the modulation periodicity, relative density of the layers, degree of roughness and chemical modulation was determined. Adding to this, AFM is a powerful tool to analyse the coating surface morphology and for accessing the level of disorder with a larger lateral validity. With this last technique we found that our coatings developed a dome-rounded surface structure, similar to zone T microstructure of Thornton's model [18], with average columnar grain diameters ranging from 90 to 120 nm.

Acknowledgements

The authors gratefully acknowledge the financial support from the French/Portuguese CNRS/ICCTI institutions (program no. 7087/1999) and from the FCT/MCT pluri-annual program.

References

[1] E.E. Fullerton, I.K. Schuller, H. Vanderstraeten, Y. Bruynseraede, Phys. Rev. B 45 (1992) 9292.
[2] K. Temst, M.J Van Bael, B. Wuyts, C. Van Haesendonck, Y. Bruynseraede, D.G. de Groot, N. Koeman, R. Griessen, Appl. Phys. Lett. 67 (23) (1995) 3429.
[3] W.-D. Münz, Surf. Coat. Technol. 58 (1993) 20.
[4] H. Holleck, V. Schier, Surf. Coat. Technol. 76/77 (1995) 328.
[5] P. Hedenqvist, S. Jacobson, S. Hogmark, Surf. Coat. Technol. 97 (1997) 212.
[6] M.F. da Silva, M.R. da Silva, E.J. Alves, A.A. Melo, J.C. Soares, J. Win, R. Vianden, in: R. Kossowsky, S. Singhal (Eds.), Surface Engineering, NATO ASI, Les Arcs, Nijhoff, 1984, p. 74.
[7] L.R. Doolittle, Nucl. Instrum. Methods B9 (1985) 344.
[8] Y.S. Gu, W.P. Chai, Z.H. Mai, J.G. Zhao, Phys. Rev. B 50 (1994) 6119.
[9] E.E. Fullerton, J. Pearson, C.H. Sowers, S.D. Bader, X.Z. Wu, S.K. Sinha, Phys. Rev. B 48 (1993) 17432.
[10] C.J. Tavares, L. Rebouta, B. Almeida, J. Bessa e Sousa, Surf. Coat. Technol. 100/101 (1998) 65.
[11] B.D. Cullity, Elements of X-Ray Diffraction, 2nd ed, Addison-Wesley, Menlo Park, CA, 1978, p. 103.
[12] C.J. Tavares, L. Rebouta, M. Andritschky, S. Ramos, J. Mat. Proc. Technol. 92/93 (1999) 177.
[13] G.M. Pharr, W.C. Oliver, MRS Bull. July (1992) 28.
[14] P.J. Burnett, D.S. Rickerby, Thin Solid Films 154 (1987) 403.
[15] F. Vaz, L. Rebouta, M.F. da Silva, J.C. Soares, J. Eur. Ceram. Soc. 17 (1997) 1971.
[16] R. Wuhrer, W.Y. Yeung, M.R. Phillips, G. McCredie, Thin Solid Films 290/291 (1996) 339.
[17] E.E. Fullerton, I.K. Schuller, Y. Bruynseraede, MRS Bull. December (1992) 33.
[18] J.A. Thornton, J. Vac. Soc. A4 (1986) 3059.